SiC-TiC nanocomposite for bulk solar absorbers applications: Effect of density and surface roughness on the optical properties

Héléne Arena, Moustapha Coulibaly, Audrey Soum-Glaude, Alban Jonchere, Adel Mesbah, Guilhem Arrachart, Nicolas Pradeilles, Marion Vandenhende, Alexandre Maitre, Xavier Deschanels

SiC-TiC nanocomposite for bulk solar absorbers applications: Effect of density and surface roughness on the optical properties

Hélène Aréna[1*], Moustapha Coulibaly[1], Audrey Soum-Glaude[2], Alban Jonchère[1], Adel Mesbah[1], Guilhem Arrachart[1], Nicolas Pradeilles[3], Marion Vandenhende[3], Alexandre Maitre[3], and Xavier Deschanels[1]

[1] ICSM, CEA, CNRS, ENSCM, Univ. Montpellier, Marcoule, 30207 Bagnols-sur-Cèze, France
helene.arena@cea.fr
xavier.deschanels@cea.fr
[2] PROMES-CNRS, UPR 8521, 7 rue du Four Solaire 66120 Font-Romeu Odeillo Via, France
[3] IRCER, UMR CNRS 7315, 87068 Limoges, France

Keywords: SiC ; TiC ; Concentrated Solar Power ; selectivity ; density ; roughness

Abstract

In this study, the potential of SiC-TiC nano-composites as solar absorbers has been studied. For solar thermal applications, materials with high solar absorptance and low emittance are ideally sought for (spectral selectivity). A semi-molecular sol-gel synthesis route leading to nanometric homogenous composites was described. The resulting SiC-TiC nanocomposite powder was sintered at different temperatures to produce samples with various relative densities (from 57 to 96 %). The samples morphology and composition were characterised by several techniques including Scanning Electron Microscopy (SEM), Energy-Dispersive X-Ray Spectroscopy (EDX), X-Ray Diffraction (XRD), carbon and oxygen elemental analyses. The link between the surface roughness and the relative density was precised and the effects on the optical properties (0.25 to 25 µm wavelength range) were studied. Comparisons were made with pure SiC and pure TiC samples with various relative densities. Overall, the sample emittance was found to strongly decrease with the increase in the relative density, leading to a great increase in the spectral selectivity, despite a little decrease in the solar absorptance. The TiC-SiC composite has an intermediate reflectance compared to the pure SiC and the pure TiC samples. With an absorptance of 0.76, an emittance of 0.44 and a selectivity of 1.74, the denser SiC-TiC could be a good candidate for bulk solar applications.

1. Introduction

The development of a sustainable, efficient and renewable energy power is a great challenge for our generation. In this context, particular attention is given to concentrating solar power (CSP) as it is a promising technology to improve the efficiency of the solar-to-electricity conversion [1, 2]. In this system, the absorber plays a key role by transferring the energy from solar radiation to a heat transfer fluid (HTF), which will be used in a thermodynamical cycle to produce electricity. However, because of thermal losses (by radiation, conduction and convection), the energy received by the absorber is not completely transferred to the HTF. As the operating temperature of the absorber is high (up to 1000°C), the main energy losses are due to thermal radiation. Indeed, when the absorber is heated, it can behave like a blackbody and emit radiation in the infrared wavelength region towards its environment. To maximize the energy efficiency, the absorber should be spectrally selective: absorbing a maximum of energy in the solar spectrum wavelength region (0.25 – 2.5 µm), while having a low thermal emittance in the IR region (above 2.5 µm), so that thermal re-radiation losses by the heated absorber are kept low [3-6]. In addition to be spectrally selective, the material constituting the absorber should be resistant to the extreme operating conditions under concentrated solar irradiation (high temperatures, oxidative/corrosive atmospheres, thermal cycles, etc.).

Nowadays, one of the materials commonly used as high temperature absorber is silicon carbide, because of its high oxidation resistance, its good mechanical properties and high sunlight absorptance [7]. However, SiC is not spectrally selective as it has a high spectral emittance [8, 9]. Transition metal carbides, nitrides and borides of column IV have been subject of many investigations due to their inherent spectral selectivity [10-24]. Among these materials, titanium carbide could be a good candidate because it is spectrally selective and it has good mechanical properties. However, it also has a low resistance to oxidation [25-32]. Previous studies showed that the combination of SiC and TiC in a nanocomposite material could be a good solution to obtain a material that is spectrally selective as well as resistant to oxidation [33].

The literature reports the combination of SiC and TiC in a composite structure to produce materials with higher relative density and improved mechanical properties (fracture toughness, Vickers hardness), thermal and electrical conductivity [34-44]. These properties are required for the absorber material as it will endure extreme operating conditions.

Several parameters have an impact on the optical properties of the materials.

First, the apparent density of the material leads to changes in the optical properties of the samples. The apparent density results from the process used for the material elaboration and corresponds to

porosity in the range of a few micrometers. Several studies indicate that the denser the material, the higher the reflectance in the whole range of wavelengths. Dense materials have a little lower absorptance (α) but above all a lower emittance (ε), thus a higher spectral selectivity which is defined as the ratio α/ε [19, 20, 23, 45-47].

Second, the surface roughness increases the absorptance of radiations in the range of wavelength lower than the average size of the holes and scratches (a few nanometers to a few hundred nanometers) [5, 6, 20, 23, 46-50]. For example, the surface patterning of zirconium boride samples by femtolaser led to better absorptance but also to higher emittance [48, 49]. The increase in the absorptance and in the emittance with the surface roughness was also noticed for SiC and TiC samples, in a preliminary study reported in Supplementary Information 1.

In most studies concerning the optical properties of UHTCs (Ultra-High Temperature Ceramics), densified or porous samples are obtained from commercial powders. To produce composites, several powders are generally mixed and sintered together. However, mechanical mixing generally induces inhomogeneities and sometimes impurities in the final composite. In the conventional process, TiC and SiC are usually synthesized by the carbothermal reduction of TiO_2 or SiO_2 with carbon black. This reaction requires high temperature (1800 – 2200°C), long reaction time (10 – 24h) and often leads to coarse-grained powders [51-53]. With nano-sized particles, the temperature (and/or time) needed for carbothermal reduction would decrease [54-58]. In addition, working with nano-sized materials would improve the homogeneity of the final products and lead to an intimate mixture of SiC and TiC particles.

Molecular routes were proposed to create proximity between the metal and the carbon source by bonding them into the same molecule. This procedure was successfully applied to SiC [59] but did not lead to a complete carbothermal reduction for TiC and SiC-TiC composites [60-62]. In addition, this route is complex and implies a thorough control of the synthesis conditions. Another way to create proximity would be to trap the carbon source in the network of a polymer material by a sol-gel process, before the carbothermal reduction. This route was applied to produce TiC, ZrC-SiC and TiC-SiC materials [63-65]. The co-condensation of the two alkoxide precursors leads to interpenetrated networks of the two oxides with enclosed carbon source particles. The carbothermal reduction produced a homogenous nanocomposite with a good repartition of both carbides and small size crystallites [66-68]. Sucrose is an interesting carbon source as it is cheap and highly soluble in several media, it was successfully used by several authors [33, 56, 57, 69, 70].

In this paper, we propose to associate SiC with TiC in a nanocomposite material for high temperature bulk solar absorber applications. We present a synthesis route where the two metal oxide precursors

copolymerize, in the presence of sucrose as the carbon source, leading to an intimate mixture. In order to improve the optical and mechanical properties, the resulting powders were sintered by Spark Plasma Sintering (SPS) to produce materials with various densities. The samples morphology and composition were characterized by several techniques including Scanning Electron Microscopy (SEM), Energy-Dispersive X-Ray Spectroscopy (EDX), X-Ray Diffraction (XRD), carbon and oxygen elemental analyses. The effects of the material relative density and of its surface roughness on the optical properties and spectral selectivity were studied by reflectance measurements in the 0.25 to 25 µm wavelength range. The results were compared to those of pure SiC and pure TiC with various densities.

2. Material and methods

2.1. Semi-molecular route

The objective was to create an intimate mixture of the two metal oxide precursors and the carbon source during the gelling. As the precursors have a different reactivity, capping agents like carboxylic acids, acetylacetone or ethylene glycol can be used to modify the surface chemistry of the precursors and lower their reactivity [71-74]. The synthesis route is described on Figure 1 and detailed in Supplementary Information 2. Titanium isopropoxide (TTIP) and tetraethyl orthosilicate (TEOS) were chosen as the source of titanium and silicon, respectively. The system was kept under inert atmosphere by nitrogen flow to prevent unintended reactions among the raw materials and water. All additions were made dropwise under continuous stirring and heating at 90°C. Because TTIP is much more reactive than TEOS, its reactivity was first lowered by complexation with citric acid dissolved in absolute ethanol. Then, TEOS was added to the mixture, followed by sucrose dissolved into water. The co-condensation was favored by the addition of sodium fluoride. The solution was first concentrated under vacuum distillation and the resulting gel was freeze dried, grounded and sifted to produce a homogeneous powder.

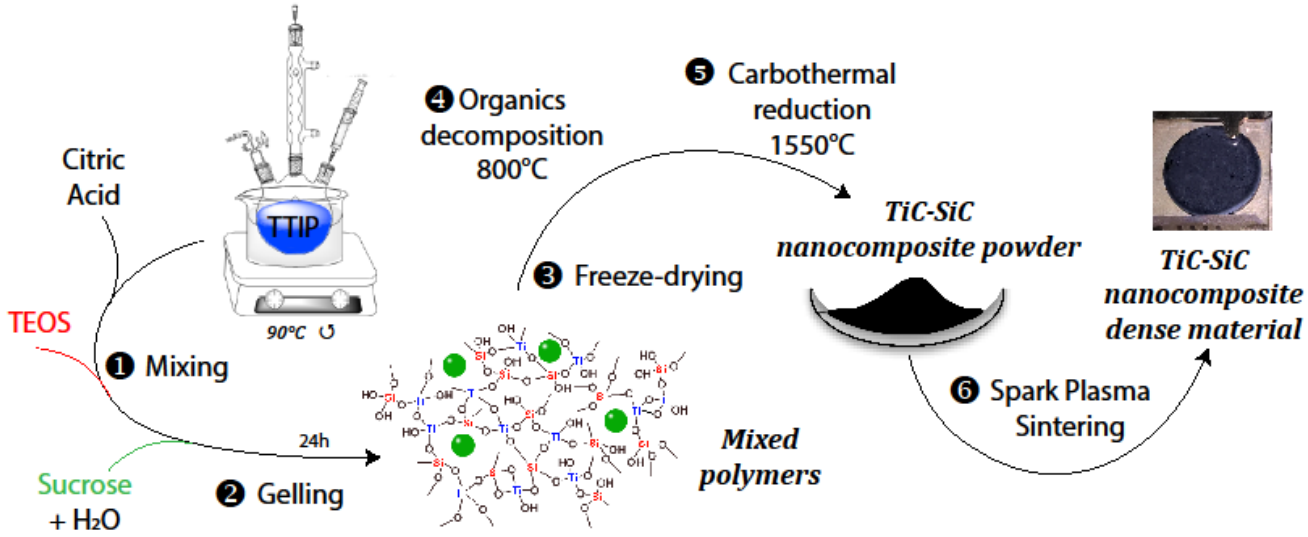

Figure 1: Reaction scheme of the synthesis route

Two heat treatments were applied under argon flow (30 $L.h^{-1}$); the first one at 800°C enabled to decompose the organic parts of the precursors (sucrose and citric acid) into carbon. According to Equation (1), the decomposition of one equivalent of sucrose could provide for a maximum of 12 equivalents of carbon. However, according to the literature, the decomposition of sucrose leads to the formation of various carbon gaseous compounds (CH_4, C_nH_{2n}, CO_2…), leaving about 48% of efficient carbon [33]. Similarly, the decomposition of one equivalent of citric acid could provide for a maximum of 6 equivalents of carbon (Equation 2). According to several studies [75-77], after the melting of citric acid at 153°C, this compound decomposes into aconitic acid and then in citra/itaconic anhydride by dehydration and decarboxylation reactions in the range of 160-270°C. At higher temperature, several gaseous compounds are formed and the proportion of residual carbon ranges between 5 and 45%. The amount of residual carbon depends on the processing parameters, heating rate especially, but also on the complexation of citric acid with metallic element [74]. When they are mixed with the other components of the synthesis, the behavior of sucrose and citric acid may be different than when they are heated alone. The second heat treatment at 1550°C led to the carbothermal reduction of oxides into carbides according to Equation 3.

Sucrose and citric acid decomposition - T = 800°C

$$\begin{cases} C_{12}H_{22}O_{11(s)} \rightarrow \mathbf{12}\ \boldsymbol{C}_{(s)} + 11\ H_2O_{(g)} & (1) \\ C_6H_8O_{7(s)} \rightarrow \mathbf{6}\boldsymbol{C}_{(s)} + 4\ H_2O_{(g)} + \frac{3}{2}\ O_{2(g)} & (2) \end{cases}$$

Carbothermal reduction - T = 1550°C

$$MO_{2(s)} + 3\ C_{(s)} \rightarrow MC_{(s)} + 2\ CO_{(g)} \qquad (3)$$

$$R = \frac{12*n_{C_{12}H_{22}O_{11}}}{3*n_{MO_2}} + \frac{6*n_{C_6H_8O_7}}{3*n_{MO_2}} \quad (4) \qquad F = \frac{n_{Ti}}{n_{Ti}+n_{Si}} = \frac{n_{TTIP}}{n_{TTIP}+n_{TEOS}} = 30\% \quad (5)$$

The ratio R (Equation 4) quantifies the carbon content resulting from the decomposition of sucrose and citric acid according to the Equations (1) and (2). Because the decomposition of sucrose and citric acid produces not only effective carbon but also carbon gaseous species, the amount of carbon available for the carbothermal reduction is not easily predictable and varies depending on the conditions. The value of the R ratio leading to a stoichiometric carbothermal reaction is empirical. According to preliminary studies, the R ratio was chosen to be 2.19 [60]. The F ratio defines the relative proportions of Ti and Si in the final material (Equation 5). The amounts of TEOS and TTIP used in the synthesis were adapted to produce a 30%at TiC – 70%at SiC composite, with an atomic F ratio of 30%.

2.2. Shaping

Sintering

To produce materials with various densities, Spark Plasma Sintering process was used on the composite powder resulting from the semi molecular route. Reference samples of pure TiC and pure SiC were also made from TiC (98%) and SiC (97.5%) powders supplied by Sigma-Aldrich with an average particle size of 3 µm and 17 µm, respectively. Sintering was conducted by Spark Plasma Sintering apparatus (Fuji-Syntex, Dr Sinter 825, Japan) under dynamic vacuum to avoid grain growth. A sufficient amount of powder was poured into a graphite die with an inner diameter of 20.4 mm. A compressive graphite foil (0.2 mm thick, Papyex©, Mersen Goup, France) was used as lubricant to coat the inner surface of the die and the surface of the punches. The powder was heated under vacuum to a maximal temperature between 1300°C to 1950°C for 5 minutes with a heating rate of 200°C/min. The heating rate was decreased at 50°C/min the last minute of heating, to avoid an overshoot. A uniaxial pressure of 75 MPa was applied upon heating. Cooling rate was 100°C/min. SPS is commonly used to sinter Ultra High Temperature Ceramics [78, 79].

Polishing

To produce mirror polished surfaces, the densified materials were polished with a Beta Buehler grinder-polisher, with SiC grinding papers and with 1 µm diamond paste (Struers) according to the procedure described in Table 1. To study the effects of surface roughness on the optical properties, the surface of several samples was scratched with SiC grinding papers with increasing grain size, the results of this preliminary study are given in Supplementary Information 1.

Polishing step	Grinding SiC paper		Rotation speed (rpm)	Time (min)
	Grit (grain/cm²)	Grain size (µm)		
1	1200	15.3	200	2
2	2000	10.3	200	5
3	4000	5	200	5 - 10
4	Diamond	1	200	15 - 20

Table 1: Polishing procedure.

2.3. Characterization methods

Optical properties

Two spectrophotometers were used to measure the total spectral reflectance of the samples. Over the wavelength range from 0.25 to 2.5 µm, the near-normal hemispherical ($R^{\perp,\cap}$) reflection spectrum was acquired with a 10 nm step using a Perkin Elmer Lambda 950 spectrophotometer. This apparatus was equipped with deuterium and tungsten lamps, PMT and InGaAs detectors, and a 150 mm integrating sphere coated with Spectralon diffuse reflective coating. The sample was illuminated at an incidence angle of 8°.

Over the wavelength range from 1.25 µm to 25 µm, the hemispherical directional reflectance ($R^{\cap,\theta}$) was recorded at different detection angles θ from 8 to 80°, using a SOC-100 HDR reflectometer (Surface Optics Corporation) coupled with a Nicolet (Fourier Transform InfraRed spectroscopy) FTIR 6700 spectrophotometer. A gold coated calibrated specular reflectance standard was used as reference during measurements (NIST calibration). The spectral range from 1.25 to 25 µm was covered by a FTIR equipped with InGaAs and DTGS/KBr detectors, coupled with Quartz and KBr beamsplitters, respectively. The sample was illuminated from all directions using a 700°C (973 K) blackbody as the infrared source and a 2π imaging gold coated hemi ellipsoid. The light reflected by the sample at a chosen detection angle was collected by a moveable overhead mirror which directed the collimated beam into the FTIR apparatus for signal treatment to retrieve the reflectance spectrum. Each reflectance spectrum was derived from 64 consecutive scans on the same sample.

The total spectral reflectance measured and the solar spectrum were interpolated over the wavelength range from 0.25 to 25 µm with a step of 2 nm to calculate the optical parameters, using Mathematica software. The solar absorptance α was calculated from room temperature measurements in the wavelength range 0.25 to 4 µm, according to Equation 6. The near-normal thermal emittance ε_ϑ (T_a) and the hemispherical emittance ε_H (T_a) at room temperature were calculated in the wavelength range 1.25 to 25 µm according to Equations 7 and 8 respectively. The hemispherical emittance represents the propensity of a surface illuminated from all directions of the hemisphere surrounding

it to reemit radiation in the same hemisphere. As reported in the results section, at room temperature and for this type of samples, the emittance calculated from near-normal reflectance measurement is representative of the hemispherical emittance. Spectral transmittance was not measured, as the samples were opaque over the whole considered spectral range.

$$\alpha = \frac{\int_{0.25\ \mu m}^{4\ \mu m}[1-R_{8°}(\lambda, T_a)]\cdot G(\lambda)\cdot d\lambda}{\int_{0.25\ \mu m}^{4\ \mu m} G(\lambda)\cdot d\lambda} \quad (6) \qquad \varepsilon_\theta(\theta, T_a) = \frac{\int_{1.25\ \mu m}^{25\ \mu m}[1-R(\lambda, T_a,\theta)]\cdot P(\lambda,T_a)\cdot d\lambda}{\int_{0.25\ \mu m}^{25\ \mu m} P(\lambda,T_a)\cdot d\lambda} \quad (7)$$

$$\varepsilon_H(T_a) = 2\int_0^{\pi/2} \varepsilon_\theta(\theta, T_a)\cdot \sin\theta \cdot \cos\theta \cdot d\theta \quad (8)$$

With λ: the wavelength [µm], $R_{8°}(\lambda,T_a)$ and $R(\lambda,T_a,\theta)$: the spectral reflectance of the sample measured at room temperature (T_a) with an illumination angle of 8° or with a variable detection angle θ, $G(\lambda)$: the standard solar irradiance spectrum (ASTM-G173 AM1.5 direct + circumsolar) [W.m^{-2}.µm], $P(\lambda,T_a)$: spectral emittance (exitance) of a blackbody at room temperature derived from Planck's law [W.m^{-2}.µm].

Porosity, density and roughness

The apparent density ($\rho_{app.}$) of the sintered samples was measured by hydrostatic weighting in pure water, using Archimedes method. Helium pycnometry measurements were conducted to determine the pycnometric density ($\rho_{pycno.}$). The theoretical density ($\rho_{th.}$) of the mixed carbide materials was calculated using a rule of mixtures taking into account the Si/Ti measured proportions and the amounts of free C and O. These densities were used to determine the relative density (D), the open and closed porosities (ϕ_{open} and ϕ_{closed}) according to the equations reported in Supplementary Information 3.

The surface roughness of the materials was measured by means of optical interferometry (Fogale Nanotech – Microsurf 3D). This apparatus gives the global roughness of a 287 µm x 481 µm area. For each sample, a least six areas were measured to obtain an average roughness value.

Morphology, composition and structure

The morphology of the samples was studied by Scanning Electron Microscopy (SEM), with an FEI Quanta 200 ESEM equipped with a Field Emission Gun. SEM images were recorded with back-scattered electrons (BSE) for composite samples and with secondary electrons (SE) for pure TiC and SiC samples. Energy Dispersive Spectra (EDX) were recorded using a Bruker SDD 5030 detector with a 123 eV resolution at the Mn (Kα) line. EDX was used to verify the composition of the synthesized products and to study the effects of oxidation.

The global Ti/Si proportion was also measured by X-Ray Fluorescence (XRF), using a Spectro-Xepos apparatus with four secondary targets (Mo, Al_2O_3, Co and HOPG Bragg crystal).

Carbon and Oxygen analyzers (LECO CS230 and ON736) were used to measure the total carbon and oxygen contents, respectively. The samples were heated under an oxygen flow for carbon analysis or in a graphite environment for oxygen analysis. In both cases, the formation of carbon oxides was detected and quantified by infrared spectroscopy, then related to the total carbon or oxygen content in the samples. Added Fe powder was used to assist the combustion in the case of carbon analysis.

The samples were characterized by X-Ray Diffraction (XRD) using the Bruker D8 advance diffractometer equipped with lynxeye detector and using Cu Kα radiation (λ=1.54184Å). Data were acquired in reflection geometry (parallel beam) in the 10-110° (2θ) or 10-90° (2θ) range of angles with steps of 0.019°. Silicon powder was collected and used as standard to evaluate the instrumental function. All the collected XRD patterns were refined by the Rietveld method with the use of the Fullprof suite package [80, 81]. TiC compound was found to crystallize in the cubic NaCl structure type in the Fm-3m space group, whereas SiC crystallizes in the ZnS structure type in the F-43m space group. During the refinement, several profile/structure parameters were allowed to vary such as zero shift, scale factor, isotropic thermal factor, unit cell parameters, moreover an anisotropic size model was applied in order to evaluate the microstructural effect. An example of the results of the Rietveld refinement obtained for the TiC compound with a relative density of 78 % is available in Supplementary Information 4.

3. Results

3.1. Characterization of the final products

All the results concerning the composition and the physical shape of the samples are reported in Table 2.

Sample	Processing parameters	Composition			Sintered materials characteristics			
	T sintering (°C)	Ti/Si proportion (%mol)	C (%mass)	O (%mass)	Relative density (%)	Open porosity (%)	Closed porosity (%)	Surface roughness (nm)
TS-57	1450	31 / 69	26.6	7.2	56.6	43.4	0	52
TS-82	1550	32 / 68	25.3	5.5	81.6	16.7	1.8	20
TS-92	1650	31 / 69	26.2	6.0	92.3	6.3	1.4	13
TS-96	1750	32 / 68	26.0	5.0	95.8	1.2	3.1	10
TiC-78	1300	100 / 0	20.0	0.67	77.9	19.1	3.0	38
TiC-91	1400	100 / 0	20.7	0.56	90.5	6.9	2.6	11
TiC-94	1500	100 / 0	19.5	0.54	94.4	2.7	2.9	17
TiC-96	1700	100 / 0	19.6	0.47	95.8	1.5	2.8	15
TiC-97	1850	100 / 0	19.6	0.46	96.6	1.1	2.4	6
SiC-72	1950	0 / 100	30.4	0.20	72.1	26.5	1.4	24

Table 2: Composition and measured characteristics of materials after SPS sintering for 5 min at P = 75MPa at the sintering temperature indicated in the table. Ti/Si proportion was obtained by average between XRF and SEM-EDX analyses. The theoretical %mass of C is 26 %, 20 % and 30 %, for TS composites, pure TiC and pure SiC samples, respectively. The error is about 0.1% for elemental analyses, relative density, and open and closed porosity. The error is about 1 nm for surface roughness and about 1%at for Ti/Si proportion.

The XRF and EDX analyses reported on Supplementary Information 5 indicate a Ti / Si proportion, respectively higher and lower than the theoretical values. Nevertheless, the average values (Table 2) are close to the theoretical ones, the synthesized composites have the expected Ti / Si proportion. The amount of C globally decreases with the increase in the sintering temperature. The amount of C is close to the theoretical value (27 %, 20 % and 30 %, for TS composites, pure TiC and pure SiC samples, respectively) and the O content is higher for the composite than for the pure TiC and SiC. This high O content could be due to a unsufficient amount of C available for the carboreduction after the sucrose decomposition at 800°C. Another explanation could be a too low temperature for the carboreduction, as the O content tends to decrease when the sintering temperature increases.

As expected, the relative density of the materials increases with the sintering temperature (Figure 2-a) [43, 82-84]. For the pure SiC sample, full relative density could not be achieved, even with a sintering temperature of 1950°C. SiC is known to be difficult to sinter because of its highly covalent bonded characteristic and the resulting low self-diffusion coefficient [85, 86].

For all samples, the open porosity decreases when increasing the sintering temperature and therby with the relative density (Table 2). In the case of the composite samples, the closed porosity increases with the sintering temperature and thereby with the relative density, while it remains constant in the case of TiC samples (Table 2). During the sintering some of the open pores are closed, leading to an increase of the closed porosity.

The relative density of all samples appear to be correlated with the surface roughness (Figure 2-b). The evolutions are almost linear for the denser materials with the exception of sample TiC-91 which shows a surprisingly low value of surface roughness (11 nm). The slope of the curve is much higher for TS composites than for the pure TiC samples, meaning that the decrease in the relative density induces a stronger increase in surface roughness for pure TiC samples. The open porosity consists in surface holes which are partly taken into account in the value of the surface roughness.

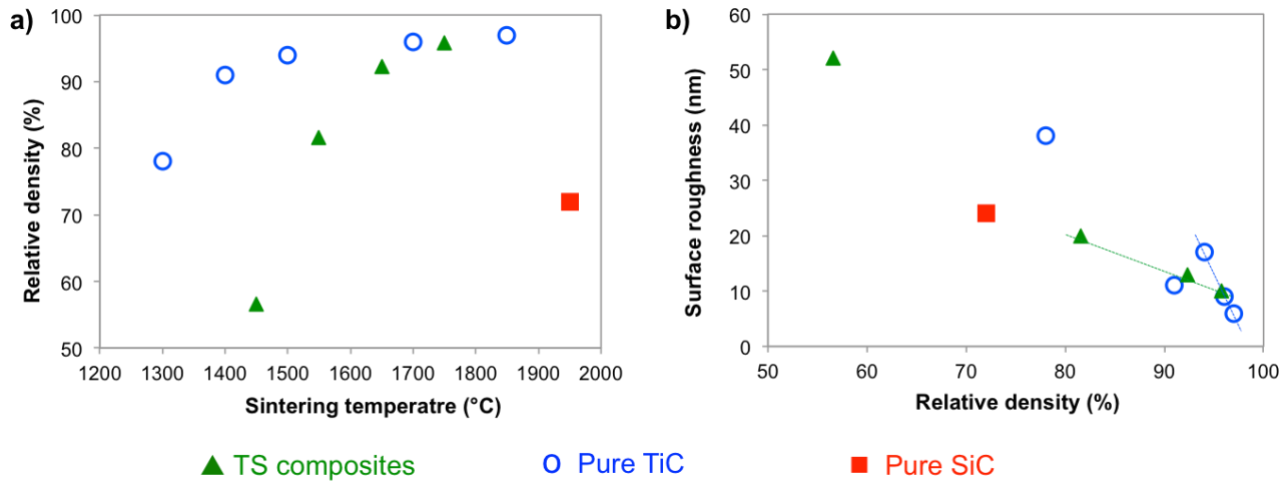

Figure 2: a) Evolution of the relative density as a function of the sintering temperature and b) evolution of the surface roughness as a function of the relative density. The dashed lines in b) are a guide for the eyes.

The morphology of the sintered materials was characterized by SEM to study the TiC and SiC grains size and distribution (Figure 3). All composites present large areas with various electronic contrasts due to changes in porosity and/or in composition. With the exception of sample TS-57, the electronic contrast between the TiC grains (white) and the SiC matrix (gray) is marked (Figure 3-b to d). The repartition of TiC grains within the SiC matrix is globally homogeneous at a short range while presenting slight variations from one area to another. The presence of open porosity is confirmed by SEM observation. The pore size is about 1 µm or lower for most samples, and several microns for the samples with the lowest densities (SiC, TS-57, TiC-78). In TS-57, it is not possible to distinguish TiC from SiC grains, the morphology of the sample surface looks like those of non sintered powders (see Supplementary Information 6) which could be due to the low relative density of the sample. In all composites excepted TS-57, the TiC grains have the same size (about 150 nm). However, when increasing the sintering temperature and thereby the relative density of the sample, the TiC grains are brought closer, forming bigger white zones with less overall porosity.

In the case of the pure SiC sample (Figure 3-e), the grains are much bigger (about 17 µm) and the open porosity is obvious. In the case of the TiC samples, the grains are smaller (about 3 µm) and the decrease in open porosity is also visible in the SEM images (Figure 3-f to j).

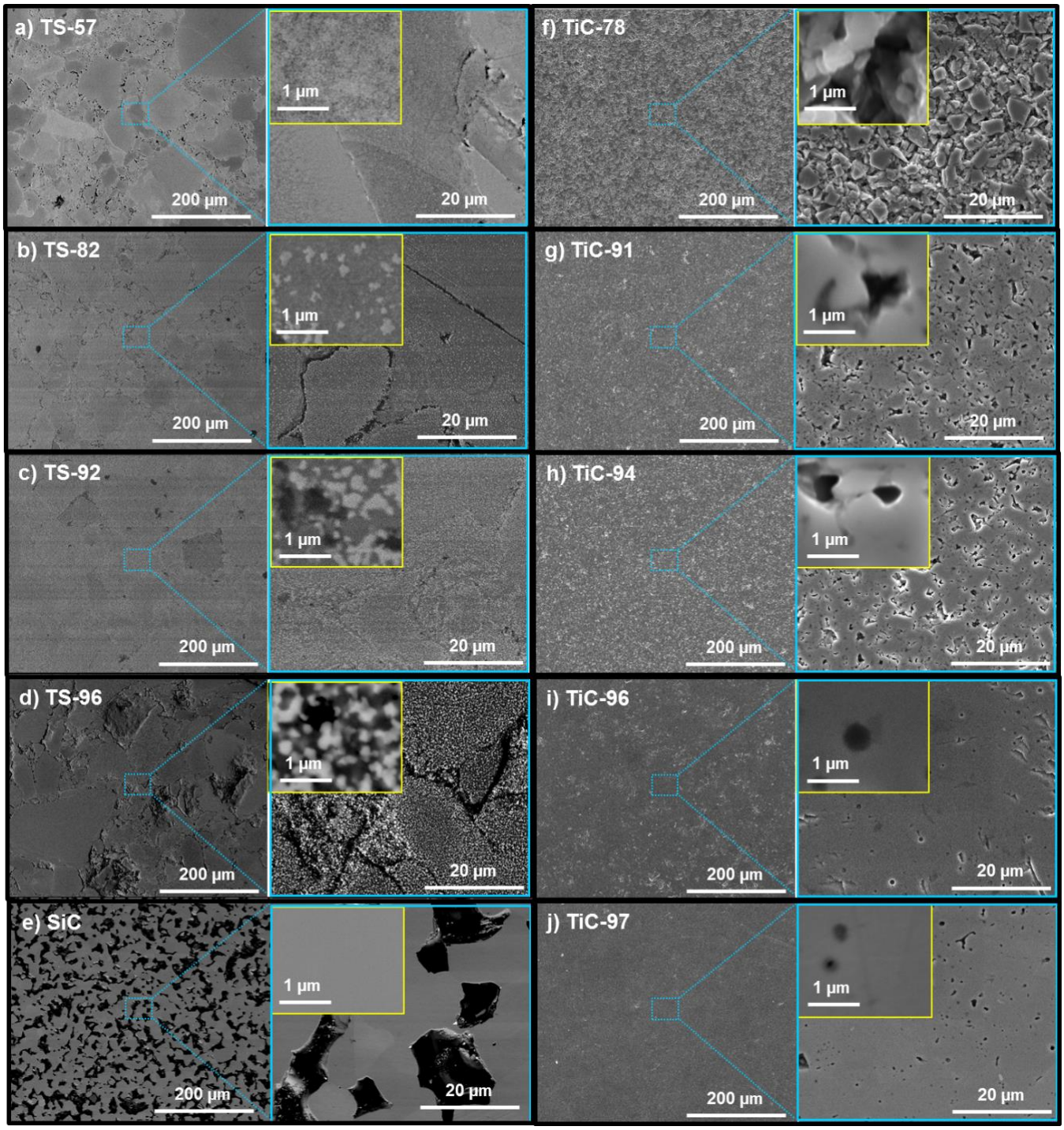

Figure 3: SEM images of the surface of the composite samples in BSE mode to show the Ti/Si distribution (a-d), the SiC reference (e) and the TiC samples (f-j) in SE mode to show the topography since there is a unique carbide phase.

After sintering, the samples were also analyzed by PXRD (Figure 4-a, b) and the results of the Rietveld refinement are presented in Figure 4-c, d) and in Table 3.

In the case of pure TiC samples, almost all the collected data showed the formation of pure and single phase. In the case of sample TiC-94, there is a reflexion around $2\theta = 10°$ which makes the Rietveld refinement impossible. From the data reported in Table 3; the obtained TiC compounds are almost free from O contamination and the O content decreases with the increase in the sintering

temperature. These results are in good aggrement with the values determined by O elemental analysis. The lattice volume of TiC is similar whatever the sample relative density and consistent with the bibliography (Figure 4-c) [87]. Unfortunately, in the pure SiC sample sintered from the commercial powder, the SiC phase cristallizes in the hexagonal system in several polymorphs which making the Rietveld refinement impossible.

In the case of the SiC-TiC composites, both TiC and SiC cubic phases are present (Figure 4-b). However, the possible incorporation of low amounts of Si in the TiC cubic structure (Ti or C sites) [88] makes the Rietveld refinement complex to interpret and it was not possible to calculate precisely the O content. The TiC and SiC unit cell parameters increase with the sintering temperature and therefore with the sample relative density (Figure 4-d). One explanation could be the elimination of the residual oxygen within the structure of both TiC and SiC phases as the sintering temperature increases.

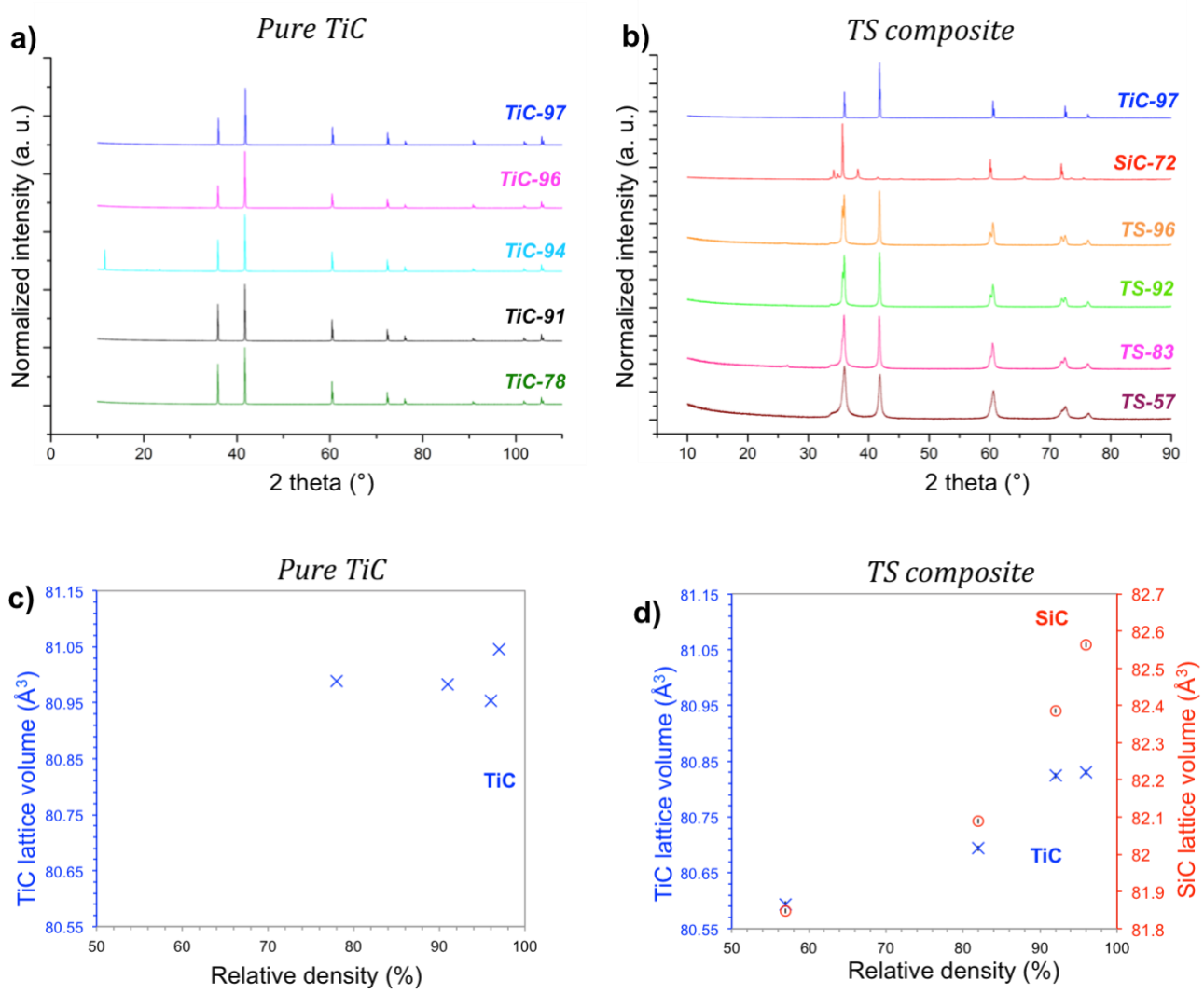

Figure 4: a, b) X-ray diffractograms of all the samples of this study and c, d) evolution of the TiC and SiC volume parameters as a function of the sample density. In c) and d), the error is about 10^{-3} Å³.

Sample	T sintering (°C)	Relative density (%)	O (%wt) elemental analysis	O (%wt) XRD	TiC lattice volume (Å^3)	SiC lattice volume (Å^3)
TS-57	1450	56.6	7.2	-	80.594	81.848
TS-82	1550	81.6	5.5	-	80.694	82.088
TS-92	1650	92.3	6.0	-	80.824	82.386
TS-96	1750	95.8	5.0	-	80.83	82.562
TiC-78	1300	77.9	0.67	0.69	80.988	-
TiC-91	1400	90.5	0.56	0.54	80.983	-
TiC-94	1500	94.4	0.54	-	-	-
TiC-96	1700	95.8	0.47	0.51	80.954	-
TiC-97	1850	96.6	0.46	0.15	81.045	-
SiC-72	1950	72.1	0.20	-	-	-

Table 3 : Data obtained by Rietveld refinement from PXRD measurements: TiC and SiC lattice volumes and O %wt. Comparison with the O %wt measured by elemental analysis.

3.2. Optical properties

To evaluate the optical properties of the samples, the total spectral reflectance was measured in the 0.25 to 25 µm wavelength range with a near normal detection (8°) (Figure 5). It appears that the reflectance of the pure TiC samples increases with the relative density, in the whole wavelength range. The effect is small between the samples with close densities (TiC-97 to TiC-91) and more marked with the less dense sample TiC-78. The reflectance of SiC is much lower than those of TiC samples and displays the characteristic peak in the 10-14 µm range. In the case of the TS composite, the reflectance curves are located between those of pure TiC and pure SiC and also display the SiC characteristic peak. The reflectance increases with the relative density of the sintered TS composite and the curves of the samples sintered at 1650°C and 1750°C (TS92 and TS96) are almost superimposed.

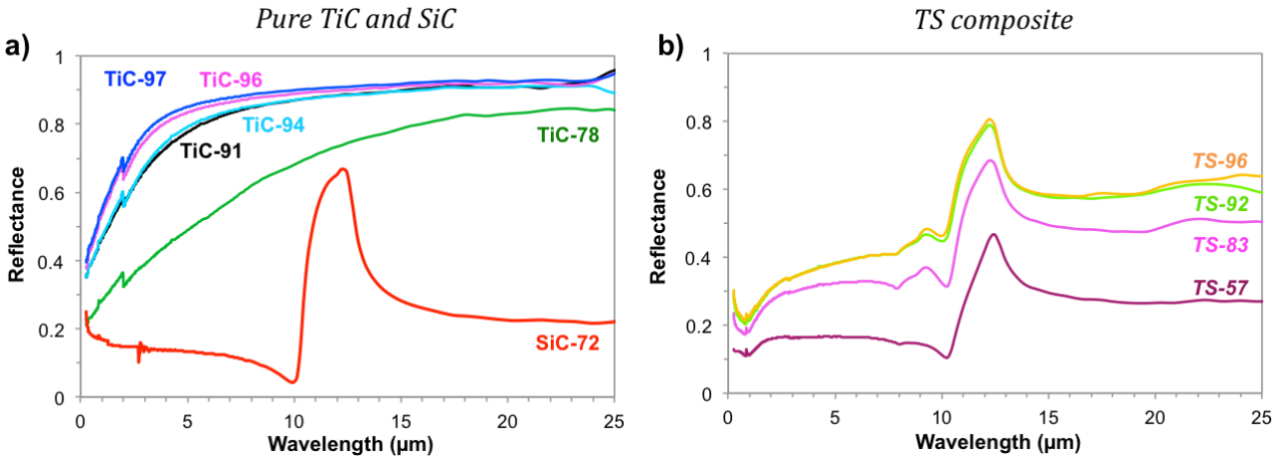

Figure 5: Evolution of the total near normal spectral reflectance for a) the pure TiC and SiC, and b) the TS composites.

4. Discussion

These materials are sought for constituting the absorber in concentrating solar power devices. In this context, they must fulfil several characteristics including good optical properties and good oxidation resistance. From the results presented above, the effects of the relative density and of the surface roughness on the optical properties are discussed below. However, the effects on the oxidation resistance were not studied here. Coulibaly et al. showed that TiC-SiC composite materials have a better oxidation resistance than pure TiC [33] and on-going work should bring new information about this topic.

Effects of the sintering temperature on the material relative density, composition and structure

The TiC samples on one hand, and the composite samples on the other hand, were sintered from the same powders (commercial product and synthesised by semi-molecular route, respectively) at a temperature ranging from 1300 to 1850°C. As presented in Table 2 and Figure 2, the relative density of the final material increased with the increase in the sintering temperature. Sintering did not induced the emergence of secondary phases, at least not in a sufficient amount to be detected by XRD (Figure 4). In the case of the composite, the sintering process did not modify the overall Si-Ti proportion (Table 2) or induce TiC grain growth. However, it favored their aggregation (in denser samples, TiC grains distribution is less homogeneous) (Figure 3). In addition, the increase in sintering temperature lowered the total O content in the final material which increased the volume of the TiC lattice towards the one obtained for the pure TiC samples. This increase in volume is consitent with the higher atomic radius of C compared to O. This result is in agreement with several studies about the evolution of lattice parameter of $TiC_xO_{(1-x)}$ oxycarbide materials as a function of the composition [87, 89].

Effects of the the material relative density on the optical properties

For both series of samples, the reflectance increases with the increase in the relative density in the whole range of analyzed wavelengths (Figure 5). From the near-normal spectral reflectance curves, the sample total solar absorptance (α), the sample total directional and hemispherical thermal emittances ($\varepsilon_{8°}$ and ε_H) have been calculated using equations (6), (7) and (8) respectively. The results are reported as a function of the sample relative density on Figure 6. As expected, the increase in the reflectance induces a decrease in both the absorptance and the emittance.

The values of hemispherical emittance calculated from multi-angle data (Equation 8) were almost the same as the values of directional emittance calculated from single near-normal reflectance curve (Equation 7), especially for SiC and the composite materials. The comparison is reported in

Supplementary Information 7. Therefore it can be remembered for further studies that at room temperature and for this type of samples, the emittance calculated from near-normal reflectance measurement is quite representative of the hemispherical emittance.

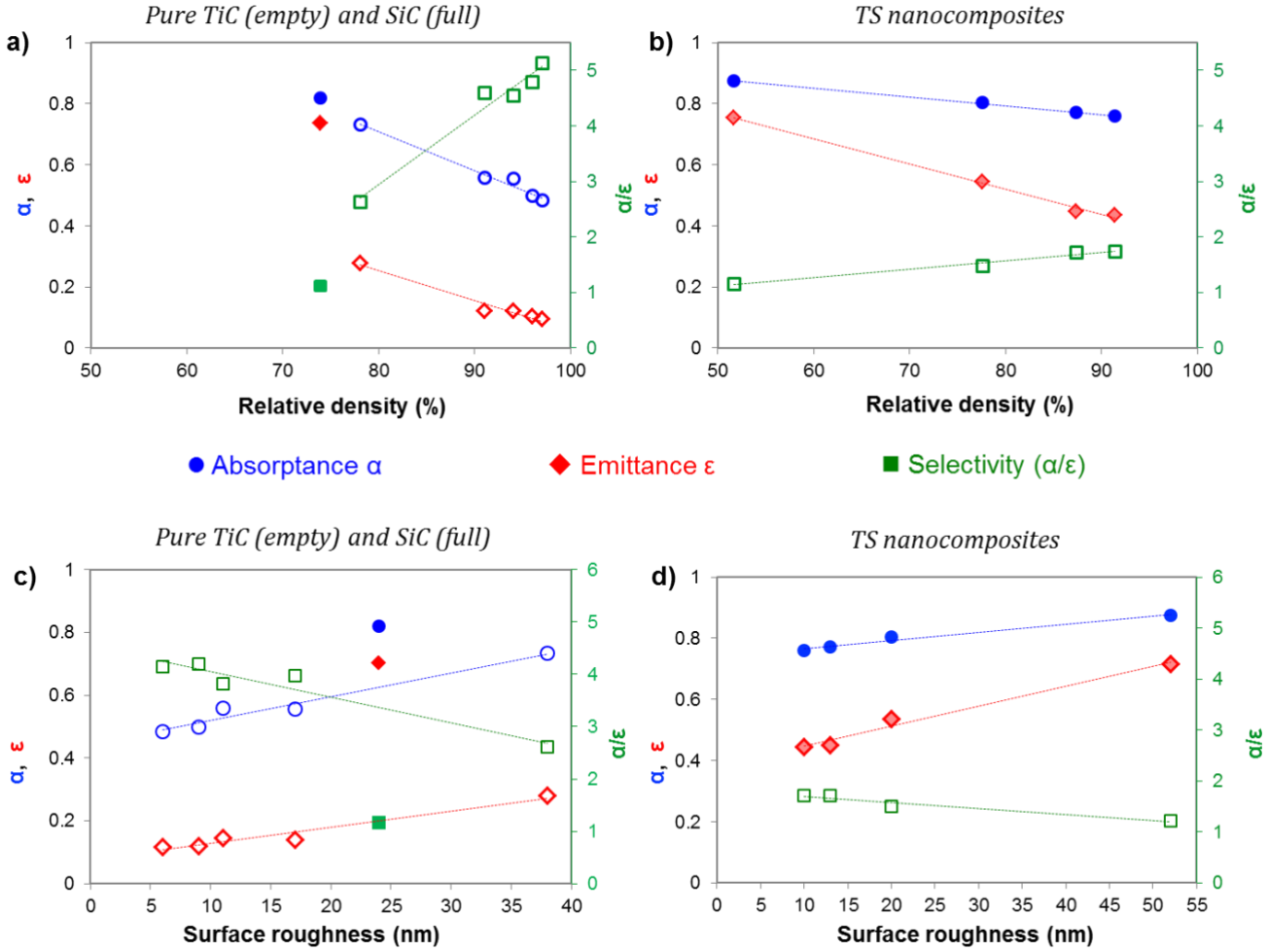

Figure 6: Evolution of the absorptance (α), the emittance (ε) and the selectivity (α/ε) as a function of (a, b) the relative density and (c, d) the surface roughness of (a, c) the pure TiC and SiC samples and (b, d) the composite samples.

For all samples, the selectivity (absorptance / emittance) increases with the sample relative density (Figure 6-a, b) and decreases with the increase in surface roughness (Figure 6-c, d). These results are consistent with those of the literature and with those of our preliminary study reported in Supplementary Information 1 [19, 20, 23, 45-47]. For TS composites, the evolution of the optical properties as a function of the relative density or of the surface roughness are almost linear. The selectivity of samples TS-92 and TS-96 is the same. The increase in absorptance with surface roughness can be explained by the multi-reflexions effect: light is trapped by the walls of the surface holes and scratches. Light is reflected several times, increasing the absorptance [5, 6, 90]. The increase in emittance is related to the increase in specific surface area as the surface roughness increases. By definition, the quantity of energy emitted by a material is proportional to its surface.

When comparing with the pure SiC and pure TiC references (Figure 6-a), it appears that all nanocomposite samples (Figure 6-b) have a higher selectivity than the pure SiC reference but lower that the one of the pure TiC reference. Due to their good spectral selectivity, these nanocomposite materials could therefore be good candidates for bulk solar applications, especially the denser ones. As TS-92 and TS-96 samples have the same value of spectral selectivity, we could consider that a SPS sintering temperature of 1650°C is sufficient to obtain a composite with interesting optical properties.

One can wonder if the effect of the sample relative density on its optical properties is only a surface effect or if the bulk has to be considered. There is a tight link between relative density and surface roughness, especially for the composite samples (Figure 2-c-d).
In the case of the composite, the two denser samples (TS-92 and TS-96) have the same spectral selectivity, their reflectanec curves are almost superimposed despite a difference in relative density of 4 % and a difference in surface roughness of 3 nm. In the case of the three denser TiC samples (TiC-94, TiC-96, TiC-97), the difference in relative density is similar (3 %) but the difference in surface roughness is much higher (7 nm), as well as the effects on the optical properties. Therefore, the effects on the optical properties seems to be mainly due to changes in surface roughness, at least for samples with a relative density higher than 90 %.

To thoroughly determine whether the closed porosity has an impact on the optical properties, the emittance should be measured directly from the non-illuminated face of the samples and not calculated from the surface reflectance curve [11]. On going work should bring new information about this question.
The key to increase the spectral selectivity is to increase the absorptance without increasing the emittance. Several ideas have been proposed in the literature, among them, the concept of directional selectivity. As the incident solar radiation is directional while the radiative losses are hemispherical, an optical cavity can be used to trap the incident solar radiation and reflect the emitted radiation back to the absorber [91]. Similarly, Hollands et al. proposed to use corrugated specular surfaces to selectively absorb the directional solar radiation while limiting the hemispherical radiation losses [50]. It could also be interesting to extend the study to higher frequencies, and monitor the properties of the SiC-TiC composites as electromagnetic wave absorber as it has been done for SiC/Si_3N composites [92, 93].

Conclusion

In this paper the potential of SiC-TiC nanocomposite materials for bulk solar absorber applications was studied. 70%at SiC – 30%at TiC nanocomposite materials were successfully synthesized by a sol-gel route from alkoxides as metal oxide precursors and sucrose as the carbon source. The carbothermal reduction was conducted at relatively low temperature (1550°C) compared to the conventional process. The resulting powder was composed of nanometric TiC and SiC particles homogeneously mixed, with 5-7 %wt of residual O. The sintering process was then adapted to produce compacts with various densities. Reference materials of pure TiC with increasing densities were also sintered from commercial TiC powder.

The spectral reflectance was measured in the 0.25 to 25 µm wavelength range to evaluate the spectral selectivity of these materials. The effects of the sample relative density and surface roughness were studied and their correlation was discussed. A tight link between the sample relative density and its surface roughness was identified and explained by considering the open porosity as the main contribution to surface roughness. The reflectance was found to increase in the whole wavelength range, with the increase in relative density and the decrease in surface roughness. Therefore, the denser and smoother the sample, the higher its spectral selectivity. The TiC-SiC composite had an intermediate reflectance compared to the pure SiC and the pure TiC samples. With an absorptance of 0.76, an emittance of 0.44 and a selectivity of 1.74, the denser SiC-TiC could be a good candidate for bulk solar applications. Even though these values are slightly lower than those obtained for other materials like ZrB_2, HfC or TaC, it should be recalled that these materials also have to be resistant to oxidation which is the case of our SiC-TiC composite [21, 33, 94]. In addition, several solutions from the literature were proposed to improve these optical properties by increasing the absorptance while maintaining a low emittance.

Acknowledgments

This work was funded by the RBPCH project from the Nuclear Energy Division of CEA and by the National Agency for Research (ANR) of the French State in the framework of the CARAPASS project (award n°ANR-16-CE08-0026) and of the French "Investments for the future" programme managed by ANR under contracts ANR-10-LABX-22-01-SOLSTICE and ANR-10-EQPX-49-SOCRATE. We wish to thank Renaud Podor and Joseph Lautru for SEM imaging, Bruno Corso for XRD assistance, Cyrielle Rey for helium pycnometry measurements and furnace assistance and Christophe Escape for his help in reflectometry measurements.

Declarations of interest

The authors declare no competing interests.

References

[1] C.G. Granqvist, Solar energy materials, Advanced Materials 15(21) (2003) 1789-1803.

[2] Y. Tian, C.Y. Zhao, A review of solar collectors and thermal energy storage in solar thermal applications, Applied Energy 104 (2013) 538-553.

[3] J. Spitz, Selective surfaces for high-temperature solar photothermal conversion, Thin Solid Films 45(1) (1977) 31-41.

[4] J. Spitz, D. Mazierebezes, Selective materials for solar-energy photothermal conversion, Journal of Optics-Nouvelle Revue D Optique 15(5) (1984) 325-332.

[5] W.F. Bogaerts, C.M. Lampert, Materials for photothermal solar-energy conversion, Journal of Materials Science 18(10) (1983) 2847-2875.

[6] C.M. Lampert, Coatings for enhanced photo thermal energy collection .1. Selective absorbers, Solar Energy Materials 1(5-6) (1979) 319-341.

[7] C.C. Agrafiotis, I. Mavroidis, A.G. Konstandopoulos, B. Hoffschmidt, P. Stobbe, M. Romero, V. Fernandez-Quero, Evaluation of porous silicon carbide monolithic honeycombs as volumetric receivers/collectors of concentrated solar radiation, Solar Energy Materials and Solar Cells 91(6) (2007) 474-488.

[8] E. Sani, L. Mercatelli, D. Jafrancesco, J.L. Sans, D. Sciti, Ultra-High Temperature Ceramics for solar receivers: spectral and high-temperature emittance characterization, Journal of the European Optical Society-Rapid Publications 7 (2012).

[9] H.H. Blau, J.R. Jasperse, Spectral emittance of refractory materials, Applied Optics 3(2) (1964) 281-&.

[10] L. Mercatelli, M. Meucci, E. Sani, Design and test of a new facility for assessing spectral normal emittance of solid materials at high temperature, in: S. Jiang, M.J.F. Digonnet (Eds.), Optical Components and Materials Xiii2016.

[11] L. Mercatelli, M. Meucci, E. Sani, Facility for assessing spectral normal emittance of solid materials at high temperature, Applied Optics 54(29) (2015) 8700-8705.

[12] E. Sani, L. Mercatelli, J.L. Sans, D. Sciti, Optical properties of black and white ZrO2 for solar receiver applications, Solar Energy Materials and Solar Cells 140 (2015) 477-482.

[13] E. Sani, M. Meucci, L. Mercatelli, D. Jafrancesco, J.L. Sans, L. Silvestroni, D. Sciti, Optical properties of boride ultrahigh-temperature ceramics for solar thermal absorbers, Journal of Photonics for Energy 4 (2014).

[14] D. Sciti, L. Silvestroni, J.L. Sans, L. Mercatelli, M. Meucci, E. Sani, Tantalum diboride-based ceramics for bulk solar absorbers, Solar Energy Materials and Solar Cells 130 (2014) 208-216.

[15] E. Sani, L. Mercatelli, J.L. Sans, L. Silvestroni, D. Sciti, Porous and dense hafnium and zirconium ultra-high temperature ceramics for solar receivers, Optical Materials 36(2) (2013) 163-168.

[16] D. Sciti, L. Silvestroni, L. Mercatelli, J.L. Sans, E. Sani, Suitability of ultra-refractory diboride ceramics as absorbers for solar energy applications, Solar Energy Materials and Solar Cells 109 (2013) 8-16.

[17] E. Sani, L. Mercatelli, D. Fontani, J.L. Sans, D. Sciti, Hafnium and tantalum carbides for high temperature solar receivers, Journal of Renewable and Sustainable Energy 3(6) (2011).

[18] E. Sani, L. Mercatelli, F. Francini, J.L. Sans, D. Sciti, Ultra-refractory ceramics for high-temperature solar absorbers, Scripta Materialia 65(9) (2011) 775-778.

[19] L. Mercatelli, E. Sani, D. Jafrancesco, P. Sansoni, D. Fontani, M. Meucci, S. Coraggia, L. Marconi, J.L. Sans, E. Beche, L. Silvestroni, D. Sciti, Ultra-refractory diboride ceramics for solar plant receivers, Proceedings of the Solarpaces 2013 International Conference 49 (2014) 468-477.

[20] E. Sani, L. Mercatelli, M. Meucci, A. Balbo, L. Silvestroni, D. Sciti, Compositional dependence of optical properties of zirconium, hafnium and tantalum carbides for solar absorber applications Solar Energy - 131(-) (2016) - 207.

[21] E. Sani, L. Mercatelli, M. Meucci, A. Balbo, C. Musa, R. Licheri, R. Orru, G. Cao, Optical properties of dense zirconium and tantalum diborides for solar thermal absorbers, Renewable Energy 91 (2016) 340-346.

[22] E. Sani, E. Landi, D. Sciti, V. Medri, Optical properties of ZrB2 porous architectures, Solar Energy Materials and Solar Cells 144 (2016) 608-615.
[23] E. Sani, L. Mercatelli, M. Meucci, L. Silvestroni, A. Balbo, D. Sciti, Process and composition dependence of optical properties of zirconium, hafnium and tantalum borides for solar receiver applications, Solar Energy Materials and Solar Cells 155 (2016) 368-377.
[24] E. Sani, M. Meucci, L. Mercatelli, A. Balbo, C. Musa, R. Licheri, R. Orru, G. Cao, Titanium diboride ceramics for solar thermal absorbers, Solar Energy Materials and Solar Cells 169 (2017) 313-319.
[25] L. Charpentier, M. Balat-Pichelin, D. Sciti, L. Silvestroni, High temperature oxidation of Zr- and Hf-carbides: Influence of matrix and sintering additive, Journal of the European Ceramic Society 33(15-16) (2013) 2867-2878.
[26] L. Charpentier, M. Balat-Pichelin, E. Beche, D. Sciti, L. Silvestroni, Microstructural characterization of ZrC-MoSi2 composites oxidized in air at high temperatures, Applied Surface Science 283 (2013) 751-758.
[27] A. Onuma, H. Kiyono, S. Shimada, M. Desmaison, High temperature oxidation of sintered TiC in an H2O-containing atmosphere, Solid State Ionics 172(1-4) (2004) 417-419.
[28] S. Shimada, A thermoanalytical study on the oxidation of ZrC and HfC powders with formation of carbon, Solid State Ionics 149(3-4) (2002) 319-326.
[29] S. Shimada, K. Mochidsuki, The oxidation of TiC in dry oxygen, wet oxygen, and water vapor, Journal of Materials Science 39(2) (2004) 581-586.
[30] M. Gherrab, V. Garnier, S. Gavarini, N. Millard-Pinard, S. Cardinal, Oxidation behavior of nano-scaled and micron-scaled TiC powders under air, International Journal of Refractory Metals & Hard Materials 41 (2013) 590-596.
[31] J. Sempere, R. Nomen, E. Serra, B. Sempere, D. Guglielmi, Thermal behavior of oxidation of TiN and TiC nanoparticles, Journal of Thermal Analysis and Calorimetry 105(2) (2011) 719-726.
[32] V.V. Rudneva, G.V. Galevskii, Investigation of thermal oxidation resistance of nanopowders of refractory carbides and borides, Russian Journal of Non-Ferrous Metals 48(2) (2007) 143-147.
[33] M. Coulibaly, G. Arrachart, A. Mesbah, X. Deschanels, From colloidal precursors to metal carbides nanocomposites MC (M=Ti, Zr, Hf and Si): Synthesis, characterization and optical spectral selectivity studies, Solar Energy Materials and Solar Cells 143 (2015) 473-479.
[34] J. Cabrero, F. Audubert, R. Pailler, Fabrication and characterization of sintered TiC-SiC composites, Journal of the European Ceramic Society 31(3) (2011) 313-320.
[35] J. Chen, W.J. Li, W. Jiang, Characterization of sintered TiC-SiC composites, Ceramics International 35(8) (2009) 3125-3129.
[36] K.S. Cho, Y.W. Kim, H.J. Choi, J.G. Lee, In situ-toughened silicon carbide-titanium carbide composites, Journal of the American Ceramic Society 79(6) (1996) 1711-1713.
[37] H. Endo, M. Ueki, H. Kubo, Hot-pressing of SiC-TiC composites, Journal of Materials Science 25(5) (1990) 2503-2506.
[38] H. Endo, M. Ueki, H. Kubo, Microstructure and mechanical-properties of hot-pressed SiC-TiC composites, Journal of Materials Science 26(14) (1991) 3769-3774.
[39] Y.M. Luo, S.Q. Li, P. Wei, L. Liu, Fabrication and mechanical evaluation of SiC-TiC nanocomposites by SPS, Materials Letters 58(1-2) (2004) 150-153.
[40] D. Shaoming, J. Dongliang, T. Shouhong, G. Jingkun, Mechanical properties of SiC/TiC composites by hot isostatic pressing, Journal of Materials Science Letters 15(5) (1996) 394-396.
[41] G.C. Wei, P.F. Becher, Improvements in mechanical-properties in SiC by the addition of TiC particles, Journal of the American Ceramic Society 67(8) (1984) 571-574.
[42] M.A. Janney, Microstructural development and mechanical-properties of SiC and SiC-TiC composites, American Ceramic Society Bulletin 65(2) (1986) 357-362.
[43] L.J. Wang, W. Jiang, L.D. Chen, S.Q. Bai, Rapid reactive synthesis and sintering of submicron TiC/SiC composites through spark plasma sintering, Journal of the American Ceramic Society 87(6) (2004) 1157-1160.

[44] M. Khodaei, O. Yaghobizadeh, H.R. Baharvandi, A. Dashti, Effects of different sintering methods on the properties of SiC-TiC, SiC-TiB2 composites, International Journal of Refractory Metals & Hard Materials 70 (2018) 19-31.
[45] D. Sciti, L. Silvestroni, L. Mercatelli, J.-L. Sans, E. Sani, Suitability of ultra-refractory diboride ceramics as absorbers for solar energy applications, Solar Energy Materials and Solar Cells 109 (2013) 8-16.
[46] D. Sciti, L. Silvestroni, J.-L. Sans, L. Mercatelli, M. Meucci, E. Sani, Tantalum diboride-based ceramics for bulk solar absorbers, Solar Energy Materials and Solar Cells 130 (2014) 208-216.
[47] E. Sani, L. Mercatelli, M. Meucci, L. Zoli, D. Sciti, Lanthanum hexaboride for solar energy applications, Scientific Reports 7 (2017).
[48] D. Sciti, L. Silvestroni, D.M. Trucchi, E. Cappelli, S. Orlando, E. Sani, Femtosecond laser treatments to tailor the optical properties of hafnium carbide for solar applications, Solar Energy Materials and Solar Cells 132 (2015) 460-466.
[49] D. Sciti, D.M. Trucchi, A. Bellucci, S. Orlando, L. Zoli, E. Sani, Effect of surface texturing by femtosecond laser on tantalum carbide ceramics for solar receiver applications, Solar Energy Materials and Solar Cells 161 (2017) 1-6.
[50] K.G.T. Hollands, Directional selectivity, emittance and absorptance properties of eve corrugated specular surfaces, Solar Energy 7(3) (1963) 108-116.
[51] E.G. Acheson, Manufacture of graphite, Google Patents, 1896.
[52] N.A. Hassine, J.G.P. Binner, T.E. Cross, Synthesis of refractory-metal carbide powders via microwave carbothermal reduction, International Journal of Refractory Metals & Hard Materials 13(6) (1995) 353-358.
[53] M.D. Sacks, C.A. Wang, Z.H. Yang, A. Jain, Carbothermal reduction synthesis of nanocrystalline zirconium carbide and hafnium carbide powders using solution-derived precursors, Journal of Materials Science 39(19) (2004) 6057-6066.
[54] V.M. Kevorkijan, M. Komac, D. Kolar, Low-temperature synthesis of sinterable SiC powders by carbothermic reduction of colloidal SiO2, Journal of Materials Science 27(10) (1992) 2705-2712.
[55] Y.J. Lin, C.P. Tsang, The effects of starting precursors on the carbothermal synthesis of SiC powders, Ceramics International 29(1) (2003) 69-75.
[56] H.P. Martin, R. Ecke, E. Muller, Synthesis of nanocrystalline silicon carbide powder by carbothermal reduction, Journal of the European Ceramic Society 18(12) (1998) 1737-1742.
[57] A. Julbe, A. Larbot, C. Guizard, L. Cot, J. Charpin, P. Bergez, Effect of boric-acid addition in colloidal sol-gel derived SiC precursors, Materials Research Bulletin 25(5) (1990) 601-609.
[58] V.D. Krstic, Production of fine, high-purity beta silicon-carbide powders, Journal of the American Ceramic Society 75(1) (1992) 170-174.
[59] X. Deschanels, D. Herault, G. Arrachart, C. Rey, A. Grandjean, G. Toquer, R. Podor, T. Zemb, G. Cerveau, R. Corriu, Comparison of two soft chemistry routes for the synthesis of mesoporous carbon/beta-SiC nanocomposites, Journal of Materials Science 48(11) (2013) 4097-4108.
[60] M. Coulibaly, Carbures nanocomposites issus de précurseurs s ol-gel et impacts sur la sélectivité optique Montpellier, 2015.
[61] K. Thorne, S.J. Ting, C.J. Chu, J.D. Mackenzie, T.D. Getman, M.F. Hawthorne, Synthesis of TiC via polymeric titanates - the preparation of fibres and thin-films, Journal of Materials Science 27(16) (1992) 4406-4414.
[62] P. Gupta, W. Wang, L.S. Fan, Synthesis of high-surface-area SiC through a modified Sol-Gel route: Control of the pore structure, Industrial & Engineering Chemistry Research 43(16) (2004) 4732-4739.
[63] S.M. El-Sheikh, Z.I. Zaki, Y.M.Z. Ahmed, In situ synthesis of ZrC/SiC nanocomposite via carbothermic reduction of binary xerogel, Journal of Alloys and Compounds 613 (2014) 379-386.
[64] J. Zhong, S.Q. Liang, K. Wang, H.T. Wang, T. Williams, H. Huang, Y.B. Cheng, Synthesis of Mesoporous Carbon-Bonded TiC/SiC Composites by Direct Carbothermal Reduction of Sol-Gel Derived Monolithic Precursor, Journal of the American Ceramic Society 94(11) (2011) 4025-4031.

[65] H. Zhang, F. Li, Q. Jia, G. Ye, Preparation of titanium carbide powders by sol-gel and microwave carbothermal reduction methods at low temperature, Journal of Sol-Gel Science and Technology 46(2) (2008) 217-222.
[66] R. Corriu, P. Gerbier, C. Guerin, B. Henner, The thermal-conversion of poly(silylene)-diacetylene metal-oxide composites - A new approach to beta-SiC-MC ceramics, Angewandte Chemie-International Edition in English 31(9) (1992) 1195-1197.
[67] R.J.P. Corriu, Ceramics and nanostructures from molecular precursors, Angewandte Chemie-International Edition 39(8) (2000) 1376-1398.
[68] R.J.P. Corriu, P. Gerbier, C. Guerin, B. Henner, From preceramic polymers with interpenetrating networks to SiC/MC nanocomposites, Chemistry of Materials 12(3) (2000) 805-811.
[69] X. Deschanels, M. El Ghazzal, C. Delchet, D. Herault, V. Magnin, A. Grandjean, R. Podor, G. Cerveau, T. Zemb, R. Corriu, Synthesis of carbide compounds derived from colloidal oxide and carbohydrate, in: S. Bucak (Ed.), Trends in Colloid and Interface Science Xxiii2010, pp. 47-52.
[70] S.T. Bae, H. Shin, H.S. Jung, K.S. Hong, Synthesis of Titanium Carbide Nanoparticles with a High Specific Surface Area from a TiO2 Core-Sucrose Shell Precursor, Journal of the American Ceramic Society 92(11) (2009) 2512-2516.
[71] C. Ang, T. Williams, A. Seeber, H.T. Wang, Y.B. Cheng, Synthesis and Evolution of Zirconium Carbide via SolGel Route: Features of Nanoparticle OxideCarbon Reactions, Journal of the American Ceramic Society 96(4) (2013) 1099-1106.
[72] D. Hanaor, M. Michelazzi, C. Leonelli, C.C. Sorrell, The effects of carboxylic acids on the aqueous dispersion and electrophoretic deposition of ZrO2, Journal of the European Ceramic Society 32(1) (2012) 235-244.
[73] S. Mahata, B. Mondal, S.S. Mahata, K. Usha, N. Mandal, K. Mukherjee, Chemical modification of titanium isopropoxide for producing stable dispersion of titania nano-particles, Materials Chemistry and Physics 151 (2015) 267-274.
[74] I.A. Mudunkotuwa, V.H. Grassian, Citric Acid Adsorption on TiO2 Nanoparticles in Aqueous Suspensions at Acidic and Circumneutral pH: Surface Coverage, Surface Speciation, and Its Impact on Nanoparticle-Nanoparticle Interactions, Journal of the American Chemical Society 132(42) (2010) 14986-14994.
[75] M.M. Barbooti, D.A. Alsammerrai, Thermal-decomposition of citric-acid, Thermochimica Acta 98 (1986) 119-126.
[76] D. Wyrzykowski, E. Hebanowska, G. Nowak-Wiczk, M. Makowski, L. Chmurzynski, Thermal behaviour of citric acid and isomeric aconitic acids, Journal of Thermal Analysis and Calorimetry 104(2) (2011) 731-735.
[77] T. Sadik, C. Pillon, C. Carrot, J.A.R. Ruiz, Dsc studies on the decomposition of chemical blowing agents based on citric acid and sodium bicarbonate, Thermochimica Acta 659 (2018) 74-81.
[78] R. Belon, G. Antou, N. Pradeilles, A. Maitre, D. Gosset, Mechanical behaviour at high temperature of spark plasma sintered boron carbide ceramics, Ceramics International 43(8) (2017) 6631-6635.
[79] G. Antou, N. Pradeilles, M. Gendre, A. Maitre, New approach of the evolution of densification mechanisms during Spark Plasma Sintering: Application to zirconium (oxy-)carbide ceramics, Scripta Materialia 101 (2015) 103-106.
[80] T. Roisnel, J. Rodriguez-Carvajal, WinPLOTR: A Windows tool for powder diffraction pattern analysis, Epdic 7: European Powder Diffraction, Pts 1 and 2 378-3 (2001) 118-123.
[81] J. Rodriguez-Carvajal, Recent advances in magnetic-structure determination by neutron powder diffraction, Physica B 192(1-2) (1993) 55-69.
[82] M. Mashhadi, H. Khaksari, S. Safi, Pressureless sintering behavior and mechanical properties of ZrB2-SiC composites: effect of SiC content and particle size, Journal of Materials Research and Technology-Jmr&T 4(4) (2015) 416-422.
[83] M. Mashhadi, M. Shambuli, S. Safi, Effect of MoSi2 addition and particle size of SiC on pressureless sintering behavior and mechanical properties of ZrB2-SiC-MoSi2 composites, Journal of Materials Research and Technology-Jmr&T 5(3) (2016) 200-205.

[84] P. Barick, D. Chakravarty, B.P. Saha, R. Mitra, S.V. Joshi, Effect of pressure and temperature on densification, microstructure and mechanical properties of spark plasma sintered silicon carbide processed with beta-silicon carbide nanopowder and sintering additives, Ceramics International 42(3) (2016) 3836-3848.
[85] N.Z. Khalil, S.K. Vajpai, M. Ota, K. Ameyama, Effect of Particle Size Distribution on SiC Ceramic Sinterability, Materials Transactions 56(11) (2015) 1827-1833.
[86] A. Lara, A.L. Ortiz, A. Munoz, A. Dominguez-Rodriguez, Densification of additive-free polycrystalline beta-SiC by spark-plasma sintering, Ceramics International 38(1) (2012) 45-53.
[87] B. Jiang, N. Hou, S. Huang, G. Zhou, J. Hou, Z. Cao, H. Zhu, Structural studies of TiC1-xOx solid solution by Rietveld refinement and first-principles calculations, Journal of Solid State Chemistry 204 (2013) 1-8.
[88] O. Tengstrand, N. Nedfors, B. Alling, U. Jansson, A. Flink, P. Eklund, L. Hultman, Incorporation effects of Si in TiCx thin films, Surface & Coatings Technology 258 (2014) 392-397.
[89] F. Réjasse, O. Rapaud, J. Léchelle, G. Trolliard, H. Khodja, O. Masson, G. Martin, A. Maître, Novel insight into the chemical analysis of light elements in oxycarbides, Acta materialia 157 (2018) 11-20.
[90] G. Pellegrini, Experimental methods for the preparation of selectively absorbing textured surfaces for photo thermal solar conversion, Solar Energy Materials 3(3) (1980) 391-404.
[91] L. Weinstein, D. Kraemer, K. McEnaney, G. Chen, Optical cavity for improved performance of solar receivers in solar-thermal systems, Solar Energy 108 (2014) 69-79.
[92] P. Wang, L.F. Cheng, Y.N. Zhang, L.T. Zhang, Flexible SiC/Si3N4 Composite Nanofibers with in Situ Embedded Graphite for Highly Efficient Electromagnetic Wave Absorption, Acs Applied Materials & Interfaces 9(34) (2017) 28844-28858.
[93] P. Wang, L.F. Cheng, L.T. Zhang, One-dimensional carbon/SiC nanocomposites with tunable dielectric and broadband electromagnetic wave absorption properties, Carbon 125 (2017) 207-220.
[94] E. Sani, L. Mercatelli, M. Meucci, A. Balbo, L. Silvestroni, D. Sciti, Compositional dependence of optical properties of zirconium, hafnium and tantalum carbides for solar absorber applications, Solar Energy 131 (2016) 199-207.